Supplementary information for:

Single-molecule-based super-resolution images in the presence of multiple fluorophores

Paul D. Simonson, Eli Rothenberg[1], Paul R. Selvin[2]

Physics Department and Center for Physics of the Living Cell, University of Illinois at Urbana-Champaign, 1110 West Green Street, University of Illinois at Urbana-Champaign, Urbana, IL 61801

[1]Present address: Department of Biochemistry, New York University School of Medicine, 550 First Avenue, MSB 363, New York, NY 10016

[2]To whom correspondence may be addressed:

Telephone: (217) 244-3371

Fax: (217) 244-7559

selvin@illinois.edu

SUPPLEMENTARY TEXT

Imaging. A typical microscope setup will include a 60-100x, high numerical aperture objective; 1.5x or 1.6x internal microscope magnification; and a sensitive EMCCD array camera. The width of a single pixel in the fluorescence image will correspond to the real, physical widths of the camera pixels divided by the total magnification of the sample. The size of the image pixel should be approximately half the width of the fluorescent spot image of a single fluorophore [1] . For example, for the experiments in this report, we used either an Olympus IX70 or IX71 microscope with a 1.45 NA 100x objective and an additional 1.5x or 1.6x internal lens (making the total magnification 150x or 160x, respectively). We used an Andor iXon (model DV8-87-E-CS-BV) or iXon+ (model DU-897E-CS0-#BV) camera with a pixel width of 16 um. This gives an effective image pixel size of 106.7 nm with 150x optical magnification, or 100 nm for 160x magnification.

Prior to acquiring data, it is useful to attempt to optimize the laser intensity and camera settings. Saturated pixels are to be avoided; however, making full use of the dynamic range of the camera is important in order to maximize signal-to-noise ratios. For EMCCD cameras, the gain should be set high enough to clearly see individual fluorophores at low density. Frame acquisition should be fast enough to be able to separate photobleaching and blinking events in time. As the density of fluorophores decreases and the average time interval between photobleaching events increases, the frame acquisition time can be increased.

Polymerizing tubulin. We prepared fresh polymerizing solution (1 mM GTP, 1 mM DTT, 50% glycerol in BRB80, pH 6.8). 2 μL biotinylated or fluorescent tubulin stock solution (20 μg/μL) was mixed with 5 μL native tubulin stock solution (10 mg/mL) on ice to prevent polymerization. 7 μL of prepared polymerizing solution was mixed with the tubulin solution. The resulting solution was incubated at 37˚C for 15-30 minutes. 86 μL centrifugation solution (20 μM paclitaxel and 1 mM GTP in BRB80, pH 6.8) was then added to microtubules and gently mixed. The solution was centrifuged at 24˚C at 15,000 g for 30 minutes. The supernatant was removed, and the pellet was resuspended in 100

μL centrifugation solution. The resulting microtubules were stored at room temperature.

***Imaging TMR-labeled microtubules* in vitro.** The starting labeling density was approximately 4:1 unlabeled:labeled tubulin monomers (Cytoskeleton, Cat. No. TL238 and TL590M). Microtubules were attached to a coverslip coated with truncated kinesin. The microtubules were excited using 532 nm laser excitation and total internal reflection fluorescence (TIRF) microscopy. Beta-mercaptoethanol (Fluka) and oxygen scavenging reagents (PCA and PCD) were used to improve fluorophore stability [2].

Imaging microtubules in cells using indirect antibody staining. COS-7 cells were seeded at low density in 35 mm glass bottom dishes and 2 mL DMEM with 10% FBS one day prior to antibody staining. The cell medium was replaced with OPTI-MEM (Gibco) 2 h prior to labeling. The medium was then removed and replaced with ~2 mL PBS. The PBS was replaced with 1 mL methanol that was stored at -20˚C. The cells were fixed 5 minutes before replacing the methanol with 2 mL PBS with 0.1% Triton X-100. The cells were washed two more times with 2 mL PBS, waiting 5 minutes between washes. The PBS was then replaced with 2 mL blocking solution (3% [w/v] BSA and 0.5% Triton X-100 in PBS, filtered using 0.22 μm syringe filter) and incubated at room temperature for 1 h. The blocking solution was then replaced with 2 mL of 1:100 dilution of DM1A anti-tubulin antibodies (Cell Signaling Technology, Cat. no. 3873S) in antibody dilution solution (0.4 g BSA and 120 μL Triton X-100 in PBS, filtered), and the cells were incubated at 4˚C overnight. In the morning, cells were washed three times with 2 mL PBS, with 5 minutes between washes. The PBS was replaced with 1 mL 1:100 dilution of secondary antibody stock solution (either CF633 conjugated goat anti-mouse [2 mg/mL, Biotium, Cat. No. 20120-F], Alexa647 conjugated goat anti-mouse antibodies [1-2 mg/mL, Cell Signaling Technology, Cat. No. 4410], or rhodamine conjugated goat anti-mouse antibodies [1-2 mg/mL, Jackson Immunoresearch Laboratories, Cat. No. 115-026-062]) in antibody dilution solution and incubated 2 h at room temperature. The cells were again washed three times with 2 mL PBS, waiting 5 minutes between washes. Finally, the PBS was replaced with 100 mg/mL PCA and 20 μL of 5 μM PCD in 2 mL PBS immediately prior to imaging. CF633 was excited using 594 nm laser

excitation in TIRF microscopy. Frames were acquired at 20 Hz, and because of the excellent brightness of the dye, we were able to use a very low EMCCD gain, which improved the dynamic range of the camera. Rhodamine was excited using 532 nm laser excitation, and Alexa Fluor 647 was excited with 633 nm excitation.

Imaging microtubules using fluorescent paclitaxel. Yellow-green fluorescent beads (Invitrogen, Cat. no. F-8787), used as fiduciary markers, were diluted in water and 12 mM HCl. The beads were flowed into a sample chamber and incubated >5 minutes. The chamber was then washed with 100 μL BRB80. 20 μL of 1 mg/mL kinesin was then added to the chamber and incubated for 5 minutes. The chamber was then washed with 100 μL BRB80, and 20 μL of microtubules diluted in BRB80 was added to the chamber and incubated for 5 minutes. Finally, 100 μL of imaging solution, consisting of 96 μL BRB80, 1 μL 700 nM Oregon Green Taxol (Invitrogen, Cat. no. P22310), 1 μL of 5 μM PCD, and 2 μL of 50 mg/mL PCA (pH 7.4), was flowed into the chamber. Imaging was done using 488 nm laser excitation. We also tried using BODIPY 564/570 paclitaxel (Invitrogen). Unfortunately, in this case we found an excessive amount of non-specific binding of the dye to the coverslip surface.

Expression and purification of streptavidin S45A. The streptavidin S45A plasmid was a gift from Patrick Stayton's lab and has been described previously [3]. Streptavidin S45A was expressed in *E. coli*, cells were lysed, and inclusion bodies were pelleted. Pellets were washed extensively, then dissolved in guanidine hydrochloride. Streptavidin was refolded and concentrated following the method of Howarth et al. [4]. In more detail:

E. coli BL21 (DE3) cells were transformed with the plasmid and grown on agar plates containing ampicillin overnight. A 15 mL overnight culture of LB with 50 μg/mL ampicillin was inoculated and grown at 37˚C with shaking. 1.5 L of LB medium and 50 μg/mL ampicillin was inoculated using the overnight culture. The culture was grown with shaking at 37˚C for 4-5 hours until OD600 = 0.7. Then protein expression was induced by adding isopropyl-β-D-thiogalactopyranoside (IPTG) to make a final concentration of 100 μg/mL. The cells were grown for another 4 h, at which point the cells were

harvest by centrifuging at 8000 g for 5 minutes. The supernatant was discarded, and the cell pellet was stored overnight at 4˚C.

The cell pellets were treated using B-PER (Thermo Scientific, Cat. no. 90078), following the manufacturer's instructions. The cell pellet was resuspended in 10 mL of B-PER. 10 mL more B-PER were added, and the solution was left to incubate 10 minutes on the bench top with occasional swirling. 100 mL of inclusion body wash buffer (50 mM TrisHCl, 0.5% Triton-X100, 100 mM NaCl, 1 mM EDTA, 0.1% [w/v] sodium azide, and 1 mM DTT, pH 8.0) was then added, and the solution was mixed well. The solution was then centrifuged at 27000 g for 10 minutes. The supernatant was discarded. The pellet was then resuspended in 10 mL of inclusion body wash buffer, and 90 mL of additional inclusion body wash buffer were added. The solution was centrifuged at 15000 g for 10 minutes. The supernatant was discarded, and the pellet was again resuspended in 10 mL plus 90 mL of inclusion body wash buffer and centrifuged. After this third wash, the pellet was resuspended in 10 mL plus 90 mL of inclusion body wash buffer that was missing Triton-X100. The solution was centrifuged again at 15000 g for 10 minutes. The supernatant was discarded. The pellet was then dissolved in 5.5 M guanidine hydrochloride in water at pH ~1.5. 250 mL of PBS was cooled to 4˚C. Using a magnetic stir bar, the PBS was stirred rapidly so that the vortex reached the top of the stir bar. The guanidine solution was then slowly added drop-wise to the fastest moving part of the solution. The stir rate was reduced, and the solution was stirred overnight at 4˚C.

In the morning, the solution was centrifuged at 17700 g for 15 minutes at 4˚C. The supernatant was then returned to stir at 4˚C while the pellet, which was assumed to contain misfolded and aggregated protein, was discarded. 62.8 g of ammonium sulfate was then added, approximately 10 g at a time, to the stirring solution. The solution was stirred at 4˚C for 3 h. The solution was then passed through filter paper (Whatman 42) using vacuum filtration. The flow-through was returned to stirring at 4˚C. 59 g of additional ammonium sulfate was added all at once to the solution. The solution continued to stir for three hours. The solution was then centrifuged at 17700 g for 15 minutes at 4˚C. The

supernatant was discarded, and the bottle was allowed to drain upside down on paper towels for approximately 2 minutes. The pellet was then resuspended in 4 mL of PBS. The solution was centrifuged at 14000 g for 5 minutes at 4˚C. The supernatant was kept while the pellet was discarded. The OD280 was then measured by using PBS as a blank and assuming 0.1 mg/mL streptavidin for OD280 = 0.355. The total yield measured in this way was 35 mg. The solution was then further diluted in PBS to a final concentration of 0.7 mg/mL and stored at 4˚C.

Imaging microtubules using streptavidin S45A. 10 μL of 1 mg/mL truncated kinesin solution was added to a flow chamber and incubated 5 minutes. 50 μL of blocking solution (50 μL 20 mg/mL casein, 1 μL 10 mM ADP in PBS) was flowed into the chamber and incubated 5 minutes. The chamber was then washed with 100 μL of 100 μM ADP in PBS, pH 8.2. 100 μL of microtubule solution (95 μL 100 μM ADP in PBS, pH 8.2; 1 μL of 20 μM paclitaxel [Cytoskeleton] in DMSO; 5 μL of solution of biotinylated microtubules) was added, and the chamber was incubated 5 minutes. 100 μL of imaging solution (100 μL 100 μM ADP in PBS, pH 8.2; 0.5 μL 5 μM [biotin]-DNA-[Atto647N]; 4 μL of 1.3 μM streptavidin S45A in 10% sucrose in PBS, pH 8.2; 1 μL of 20 μM paclitaxel [Cytoskeleton] in DMSO) was then added. Atto647N was imaged using 633 nm laser excitation in TIRF microscopy with a 0.5 s frame acquisition time.

The [biotin]-DNA-[Atto647N] construct consisted of the following two single strands of DNA, annealed together:

[Atto647N]-TGGCGACGGCAGCGAGGCTTTTTTTTTTTTTTTTTT

[Biotin]-GCCTCGCTGCCGTCGCCA

Simulating fluorophores. For a single frame, fluorophores were simulated by plotting Gaussian functions, integrated over the area of single pixels. Various levels of a flat background value were then added. Finally, Poissonian noise was added to the frame using the Poisson distribution function in the GNU Scientific Library (GSL).

For multiple frames and dynamic fluorophore simulations, fluorophores were allowed to switch

between fluorescing, temporarily inactive, and permanently photobleached states. Unless otherwise stated, if a fluorophore switched states, the time of occurrence of the transition during the course of the simulated frame acquisition was chosen randomly as any time within the course of the frame. The intensity of the fluorophore within that given frame was reduced according to the fraction of the frame acquisition time during which the fluorophore was simulated to be inactive.

The probability of switching to a different was simulated by calculating switching probabilities that corresponded to the transition rates between the given possible states. For our simulations, we limited ourselves to states corresponding to fluorescing, temporarily inactive states, or permanently photobleached states. The simulated frame acquisition time was chosen to be longer than the lifetime of any of the possible states.

Spot (fluorophore transition event) detection algorithm. We used the following algorithm to automatically detect spots in the backwards-subtracted movie that correspond to photobleaching events:

1. Dilate the image. To dilate the image, each pixel's intensity value is replaced with the greatest intensity value of the eight nearest neighbors, or it is unchanged if the pixel intensity is greater than that of any one of the eight nearest neighbors. The image might have to be dilated twice (i.e., apply this step twice) for very low signal to noise ratios.
2. Find the positions of all pixels that were not affected by the dilation. These are the local maxima.
3. Determine the average pixel intensity of all pixels within the radius R (usually R is chosen to be three pixels) of a given local maximum.
4. Compare this with a chosen threshold value T (see below). Local maxima with values that are above the chosen threshold are considered as potential "real" fluorophore photobleaching events.
5. An output TIFF file is produced that can be compared with the original image file to check spot detection performance.

Spots corresponding to photoactivation events, which appear darker than background in the backwards-subtracted image, are detected in a very similar way, except in this case we look for local minima.

The choice of threshold value T can be made by first calculating the expected value of the spot's average pixel intensity. This can be estimated by using

$$I_{API} = \frac{\int_0^R A \exp(\frac{-r^2}{2\sigma^2}) 2\pi r \mathrm{d}r}{\pi R^2} \tag{S1}$$

where σ characterizes the width of the two-dimensional Gaussian function and A is the peak intensity of the Gaussian function. It can be noted that A is related to the total expected number of photons, I_0 by

$$I_0 = 2A\pi\sigma^2. \tag{S2}$$

Since the fluorophore can photobleach anytime during the acquisition of a single frame, the threshold is chosen to be half the value of I_{BSA} so that the threshold intensity is far enough below the expected photobleaching intensity so as to not miss steps. For real data, setting an even lower threshold can be advantageous (although single photobleaching events might be mistaken as two sequential photobleaching events) since this essentially will reduce the amount of frame averaging performed when, for example, nearby fluorophores go into metastable dark states for only a fraction of a frame. These fraction-of-a-frame events, if significant, have the potential to introduce additional error if not identified.

If the peak intensity and spot width of single fluorophores are not known *a priori*, the threshold can still be chosen by inspecting a small number of frames near the end of the backwards-subtracted movie where individual fluorophore transitions are more obvious. The investigator can try threshold values until apparent transitions are identified or just start with a "ballpark" guess. The median peak intensities and spot widths that are identified after fitting to Gaussian functions (see below) can then be used to estimate what an appropriate detection threshold value should be before analyzing the entire data set.

To reduce the probability of treating two fluorophores that simultaneously photobleach as one, our analysis software also enables the user to set a maximum spot intensity threshold. Spots with high intensity values are likely to correspond to multiple fluorophores that simultaneously photobleach (or photoactivate). Spots that pass this threshold are recorded for purposes of calculating frame averaging ranges, but they are not used themselves for localizing their associated fluorophore events with Gaussian functions. We find 1.5 I_{API} to be a reasonable upper threshold. Unfortunately, we currently have no method for detecting simultaneous photobleaching and photoactivation events that overlap in space.

Probability of detecting false positives during spot detection. In the case of no fluorophore transition event in the backwards-subtracted image, the expectation value of the associated pixels is zero; however, due to shot noise and camera noise, the actual pixel intensities fluctuate around zero. Thus, for large fluctuations, there is the possibility of detecting false positives in the spot detection process. The actual average intensity of the N local pixels will be

$$I_{API} = \frac{\sum_{n=0}^{N} I_n}{N} \tag{S3}$$

where I_n is the intensity of the nth pixel. The variance of the sum can similarly be estimated by [5]

$$\sigma_{API}^2 = \frac{\sum_{n=0}^{N} \sigma_n^2}{N^2} \tag{S4}$$

If the standard deviations of each pixel σ_n all equal σ, then eq. (S4) reduces to the more familiar

$$\sigma_{API}^2 = \frac{\sigma^2}{N}. \tag{S5}$$

The probability that N random pixels will have an average pixel intensity I_{API} greater than the spot detection threshold T (appearing as a photobleaching event) or less than $-T$ (appearing as a photoactivation event) is then simply

$$P(I_{API} < -T \cup I_{API} > T) = 2\int_{T}^{\infty} \frac{1}{\sigma_{API}\sqrt{2\pi}} \exp\left(\frac{-x^2}{2\sigma_{API}^2}\right) \mathrm{d}x. \tag{S6}$$

For a numerical example, consider a flat, expected background pixel intensity of 10000 photons.

The variance of each pixel in the backwards-subtracted movie will be 200 photons^2, considering only shot noise. If the spot detection integration radius is 3 pixels, then 29 pixels total will be averaged, and σ^2_{API} is approximately 6.9 photons^2. If we set T = 20 photons, then the probability of finding a false positive is 0.4%.

If in the other extreme case the local maximum to be tested is centered on a Gaussian spot with peak intensity = 10000 photons, spot diameter ≈ 2.6 pixels, and no other fluorescent background, then since the sum of Poissonian variables gives a new Poissonian variable,

$$\sigma^2_{API} \approx \frac{2\int_0^3 10000 \exp\left(\frac{-r^2}{2\times 1.3^2}\right) 2\pi r \mathrm{d}r}{29^2} \approx 235 \tag{S7}$$

For T = 20, probability of finding a false positive in this case is 19% and does not drop to <1% until T > 39.5 photons. To detect an actual photobleaching event for such a background, however, the expected average pixel intensity for a fluorophore with peak intensity = 500 photons (making 20 fluorophores total in the composite spot) would be 170 photons. We could therefore expect to easily choose a threshold value that is efficient at detecting transitions ($T \leq$ 85 photons) but have less than 1% false positives (T > 39.5 photons). Similarly, for the case of 40 fluorophores contained in the Gaussian spot (each with peak intensity = 250 photons) 39.5 < T < 42.5.

Of course, detected false positives found with the spot detection algorithm will not necessarily result in equal numbers of additional spots plotted in the final super-resolution image since frame averaging will occur (if possible) before the Gaussian fitting step, and the resulting Gaussian fit must pass the rejection criteria (width, ellipticity, intensity, etc.) before a spot is plotted.

Weighted two-dimensional, elliptical Gaussian fits using least-squares estimators and Levenberg-Marquardt fitting. The noise is governed by (1) the dark noise due to the camera in the pre-event image, (2) the shot noise in the pre-event image, (3) the shot noise in the post-event image, (4) the dark noise in the post-event image, and (5) intrinsic fluctuations in the amount of fluorescence from the fluorophores themselves. Because one frame is subtracted from another, the standard deviations of the

individual pixel intensities add in quadrature to give the total pixel noise of the resulting subtracted image [6]. The total noise associated with a single pixel in the final subtracted image (difference of frames k and [k + 1], or in the case of frame averaging, the difference of the average of frames [$k - N_B + 1$] through k and the average of frames [$k + 1$] through [$k + N_A$]) can be estimated by

$$\sigma = \sqrt{\frac{\sigma_{A,shot}^2}{F_A} + \frac{\sigma_{A,dark}^2}{F_A} + \frac{\sigma_{B,shot}^2}{F_B} + \frac{\sigma_{B,dark}^2}{F_B}} \tag{S8}$$

where $\sigma_{A,shot}$ is the shot noise associated with the pixel in the frames after a photobleaching event, $\sigma_{A,dark}$ is the associated dark noise in the frames after photobleaching, and F_A is the number of frames after the photobleaching event that are averaged. By replacing the A with B in these terms, the corresponding values are represented for the frames before photobleaching. In our software, we estimate $\sigma_{A,shot}$ as the square root of the pixel intensity (after subtracting the camera baseline count) of the frame-averaged image. $\sigma_{A,dark}$ is estimated by selecting a portion of the image in which there are no fluorophores present and finding the standard deviation of the pixel intensities. $\sigma_{A,dark}$ is assumed to be equal to $\sigma_{B,dark}$. If the electron-multiplying gain (EM gain) is used on an EMCCD camera, σ is multiplied by sqrt(2).

The Gaussian fit is done by fitting all pixels within a given radius of the brightest pixel of the spot using Levenberg-Marquardt fitting (using the GNU Scientific Library). For simulated fluorescent spot data with a spot width of 3 pixels and 700 counts peak intensity on a flat background (with added noise), the spot fitting accuracy did not increase significantly past a fitting radius of 3 pixels. For fitting the real data, we used a fitting radius of four pixels for the Gaussian fitting. The individual pixels are weighted according to the estimated noise associated with each pixel. Using a weighted Gaussian fit reduced fit error by about 10% for the simulated single spots on dark, uniform backgrounds. It was therefore concluded that the improvement in fitting accuracy would be improved by at least 10% for a non-uniform background. The fitting accuracy is reported as the error reported by the fitting program using the covariance matrix of the best fit parameters. For simulated spots on dark backgrounds, the

errors were found to be very near the fitting accuracy predicted by Thompson et al. for single spots on flat backgrounds [1]. However, we do not estimate the error using the Thompson et al. equation but, rather, use the error reported by the fitting program, since the Thompson et al. error equation is derived by assuming a flat background with Gaussian noise. Using the error reported using the fitting program gives the added benefit that we do not have to know the counts-to-photons conversion factor, which is required by the Thompson et al. equation, in order to calculate the localization error.

Gaussian fitting using maximum likelihood estimators and Fisher score fitting. As an alternative to fitting with least-squares estimators and Levenberg-Marquardt fitting using GSL, we later wrote our own fitting algorithm based on maximum-likelihood estimators and the Fisher scoring method [7, 8]. The intensity value of a single pixel with indices (i, j) is the intensity of the two-dimensional Gaussian function integrated over the area of the pixel. This was expressed by

$$g(i,j;\theta) = \int_i^{i+1}\int_j^{j+1} A\exp\left(-\frac{(x-x_0)^2}{2\sigma^2}\right)\exp\left(-\frac{(y-y_0)^2}{2\sigma^2}\right)\mathrm{d}y\mathrm{d}x = \frac{1}{2}\pi A\sigma^2\Delta E_x(i)\Delta E_y(j) \tag{S9}$$

where θ is the vector of parameters

$$\theta = (A\ x_0\ y_0\ \sigma)^{\mathrm{T}} \quad ; \tag{S10}$$

and A is the peak intensity, (x0, y0) is the center of the Gaussian function, σ relates the width of the Gaussian function, and

$$\Delta E_x(i) \equiv \mathrm{erf}\left(\frac{i-x_0}{\sqrt{2}\sigma}\right) - \mathrm{erf}\left(\frac{1+i-x_0}{\sqrt{2}\sigma}\right) \tag{S11a}$$

$$\Delta E_y(j) \equiv \mathrm{erf}\left(\frac{j-y_0}{\sqrt{2}\sigma}\right) - \mathrm{erf}\left(\frac{1+j-y_0}{\sqrt{2}\sigma}\right) \quad . \tag{S11b}$$

The fitting error estimates were expressed using the Cramér-Rao lower bound (CRLB), which gives the lower bound of the variance of any unbiased parameter estimator [7, 8]. The CRLB variances of the individual parameter estimates are the corresponding diagonal elements of the inverse Fisher

information matrix [7]. For normally distributed observations (recorded pixel intensities), the elements of the Fisher information matrix are given by

$$f_{pq} = \sum_{n=0}^{N} \frac{1}{\Delta g_n^2} \frac{\partial g_n(\theta)}{\partial \theta_p} \frac{\partial g_n(\theta)}{\partial \theta_q} \tag{S12}$$

where N is the total number of pixels used in the Gaussian fitting, $g_n(\theta)$ are the expectation values of the pixels with varying indice (i, j), and Δg_n^2 is the estimated variance of the pixel (see eq. [S1]). We note that although photon detection is a Poissonian process, because we are averaging frames, subtracting frames, including camera dark noise (readout noise), and multiplying by factors according to the EM gain setting in the camera, the noise associated with a given pixel is no longer Poissonian, which is why we have elected to use the normally-distributed Fisher information matrix. In form, however, the calculations of the Fisher information matrices for the two cases are nearly identical.

The fitting algorithm has the following form:

1. Starting guess parameters are chosen based on the pixel with maximum intensity in order to guess A (where A = max. intensity – min. intensity), x_0, and y_0. σ is initially guessed to be 1.3 pixels.
2. In the Fisher scoring iterative fitting procedure, the iteration step of the fit parameter vector is given by [7]

$$\Delta\theta_{FS} = F_\theta^{-1} s_\theta \tag{S13}$$

where F_θ^{-1} is the inverse Fisher information matrix for parameter estimate vector θ and s_θ is the Fisher score, the kth element of which is given by [7]

$$s_{\theta_k} = \sum_n \frac{\partial g_n(\theta)}{\partial \theta_k} \frac{w_n - g_n(\theta)}{\Delta g_n^2} \tag{S14}$$

where w_n are the observed pixel values. $\Delta\theta_{FS}$ is reduced in magnitude if it will result in one or more of the parameters becoming negative.

3. If the magnitude of the step is less than the chosen tolerance (0.0001), then the algorithm has

reached convergence.

4. The parameters are then updated to $\theta_c = \theta + \Delta\theta_{FS}$.
5. If convergence was not reached and the maximum allowed number of iterations was not reached, then return to step 2.

We tested the accuracy and reported fitting error of the fitting algorithm as implemented in the gSHRImP analysis software under two types of cases using simulated data.

In the first case, a fluorophore was simulated to blink on and off with varying levels of background. The expected amount of background was chosen to be the same for each pixel, making a flat (before noise was added) background. The fluorophore was repeatedly turned on and off, one transition per frame, and the situation was made ideal by generating the data such that transitions occurred in between frames (i.e., the expected fluorescence in a given frame was either 0% or 100% of expectation, nothing in between). The fluorophore was positioned at the center of a pixel [where localization accuracy is expected to be poorest—see [9]] in the center of a 21x21 pixels^2 frame. The peak intensity, A, of the fluorophore was chosen to be 500 photons, and the width value, σ, was chosen to be 1.3 pixels. 1001 frames were simulated. The background value was chosen to vary between 0 and 20000 photons. The standard deviation of the x0 estimates matched well with the algorithm's reported CRLB estimates of the error, until the background approached approximately 14000 photons. Unfortunately, it was noticed that the spot detection algorithm seemed to start to fail significantly near a background of only 7500 photons, detecting too many spots (500 photobleaching events and 500 photoactivation events are the expected values), which also resulted in fewer good spot localizations. Improving the spot detection algorithm will be an ongoing area of research. Finally, we note that we also calculated what the Thompson et al. estimated error [1] would be for the given background values and found, similar to [8], that the Thompson equation uniformly estimated a lower error compared to the CRLB error estimate. See Table S6 for the first case's results.

In the second case, we were interested in the effect of a non-uniform background. We proceeded in

the same way as in the first case, but we fixed the background at 100 photons per pixel and added a second fluorophore that was shifted 0.25 pixels along the *x* axis, relative to the first fluorophore. Shifting was done in an effort to see whether the estimated position of the first fluorophore could be biased in the direction of the second fluorophore. This second fluorophore was not allowed to blink, and its peak intensity was varied between 0 and 50000 fluorophores. In this case, the spot detection algorithm performed quite well for all peak intensity values of the second fluorophore tested. The estimated errors calculated using the CRLBs also corresponded quite well with the actual standard deviations of the x_0 estimates from the center of the pixel. There was no apparent biased shifting of the x_0 estimates in the direction of the second fluorophore. We also note, if the peak intensity of the second fluorophore is divided by 500 to give a number for simulated nearby fluorophores, the error associated with localizing the first fluorophore showed the expected increase with respect to the square root of the number of nearby fluorophores (graph not shown). See Table S7 for numerical results.

Estimation of the effect of nearby fluorophores. As a simple way to get a sense of the effect of added background fluorescence due to nearby fluorophores, we can temporarily assume that the background is flat and make use of the results of Thompson et al. for estimating the localization error [1, 2],

$$\sigma_i = \sqrt{\frac{s^2 + a^2/12}{N} + \frac{8\pi s^4 b^2}{a^2 N^2}} \tag{S15}$$

where σ_i is the estimated localization error along the *x* or *y* direction; *s* is half the spot width along the given direction; *a* is the length of the pixel; *N* is the number of photons collected from the fluorophore in a single frame; and *b* is the background noise per pixel, in terms of photons. Let us suppose that we have *m* fluorophores distributed randomly in an area $A = 4s^2$, which is roughly the size of the area of a diffraction-limited spot, and each fluorophore emits *N* fluorophores per movie frame. Let us further assume that there are enough fluorophores to make the fluorescence intensity roughly constant within the area *A*, and the background photon counts due to dark currents, etc., are negligible compared to the photons collected from the fluorophores. In this case, assuming the noise associated with detecting

photons is Poissonian, b is approximately

$$b = \frac{\sqrt{mN}}{\sqrt{A}/a} = \frac{\sqrt{mN}}{2s/a} = \frac{a\sqrt{mN}}{2s} \tag{S16}$$

Now let us suppose that a single fluorophore photobleaches in the transition from one frame to the next. What is the estimated accuracy that can be achieved if we apply gSHRImP and do no frame averaging? The number of fluorophores left after the photobleaching event that will contribute to the background fluorescence is now (m – 1). However, the shot noise due to the background fluorophores doubles since the spot image we fit to a Gaussian is actually the difference of two frames, the background noise in both frames should be equivalent, and the background noise due to each frame adds in quadrature (see Equation [S1]). Using our expression for b, the localization error can then be estimated as

$$\sigma_i = \sqrt{\frac{s^2 + a^2/12}{N} + \frac{4\pi s^2 (m-1)}{N}} \tag{S17}$$

Thus, if m = 10, s = 125 nm, a = 100 nm, and N = 10,000, then σ_i = 13 nm. It should be noted that in Equation (S4), the last term in the square root dominates even for small values of m (i.e., m > 1), so the localization error can be expected to increase as the square root of (m - 1). It should also be noted that this equation does not account for fluctuations in N from individual fluorophores, which will further increase the localization error. Of course, localization accuracies can be improved if frames can be averaged (see Equation [S1]). If F is the number of frames that can be averaged before and after the photobleaching event, then Equation (S4) decreases to

$$\sigma_i = \sqrt{\frac{s^2 + a^2/12}{N} + \frac{4\pi s^2 (m-1)}{FN}} \tag{S18}$$

For theoretical localization accuracies for other values of nearby spots and frames averaged, see Fig. S5.

As an example of the density of fluorophores that can be used and yet still find acceptable localizations of spots, we consider the super-resolution images produced by imaging the photobleaching of *in vitro* microtubules labeled with TMR. If the number of fluorophores localized is plotted as a

function of frame, we see that the number starts out low, increases to a peak, and then steadily decreases (see Fig. S1a). The starting, low number of spot localizations can be explained by assuming that the microtubules are overly labeled with fluorophores. As the fluorophores photobleach, the density of active fluorophores decreases, and the ability to localize spots increases until a best fluorophore density is reached. The fluorophores then continue to photobleach so that the number of fluorophores localized per frame begins to decrease because the system is running out of available fluorophores. By knowing the average fluorescence output per frame of a single fluorophore, the total number of fluorophores per length of microtubule can be estimated. In Fig. S1a, the maximum fluorophores-localized-per-frame occurs at a fluorophore density of one fluorophore per 14 nm of length of microtubule.

Fluorophore density limits based on photobleaching and blinking rates. Of course, even if the potential localization error is acceptable for a given high density of background fluorophores based simply on flourophore emission intensities, the dynamics of the photobleaching and blinking also affect the maximum possible density. That is, if the fluorophores near-simultaneously photobleach, blink, etc., and they are spatially close, then the fluorophores cannot be localized via gSHRImP, even if their brightness is otherwise sufficient to localize fluorophores to good accuracy.

To get a sense of how the photobleaching rate affects the maximum useful fluorophore density, consider the following. Assume that we have N fluorophores within a radius R where R is the minimum distance between photobleaching events and Δt is the minimum time required between photobleaching events (Δt will be dependent on the frame acquisition time and the required number of photons for achieving the desired localization accuracy). Further assume that at least 90% of the time, we want the time between subsequent photobleaching events to be $\geq \Delta t$. Let τ_{pb} be the photobleaching lifetime of the fluorophore. Then, the probability that an individual fluorophore will photobleach within a time interval Δt is given by

$$\lambda_{pb} = 1 - \exp(-\Delta t/\tau_{pb}). \tag{S19}$$

The probability that *none* of N fluorophores photobleach within Δt is then given by a binomial

distribution

$$P(0|N,\lambda_{pb}) = \binom{N}{0}\lambda_{pb}^{0}(1-\lambda_{pb})^{N} = (1-\lambda_{pb})^{N}. \tag{S20}$$

The probability that only one photobleaches in Δt is

$$P(1|N,\lambda_{pb}) = \binom{N}{1}\lambda_{pb}^{1}(1-\lambda_{pb})^{N-1} = N\lambda_{pb}(1-\lambda_{pb})^{N-1}. \tag{S21}$$

The probability that *only one* photobleaches in a frame given that *at least one* photobleached in the frame is simply

$$\frac{P(1|N,\lambda_{pb})}{1-P(0|N,\lambda_{pb})}\ . \tag{S22}$$

To extend the arguments to fluorophores that both photobleach and blink is straightforward. In this case, τ_{pb} is replaced by the lifetime associated with transitioning to a permanently photobleached state *or* a temporarily inactivated state,

$$\tau_N = \frac{1}{k_{pb}+k_{pi}} = \frac{1}{\frac{1}{\tau_{pb}}+\frac{1}{\tau_{pi}}} \tag{S23}$$

where k_{pb} is the photobleaching rate and k_{pi} is the rate of transitioning to the temporarily inactive state. The probability λ_N that an individual fluorophore photobleaches or temporarily inactivates within Δt is then calculated following Eq. S19. Assume further that there are M fluorophores in the temporary inactive state that can transition to the fluorescing state at a rate $k_M = 1/\tau_{pa}$. The joint probability that neither (1) a fluorescing fluorophore photobleaches or transitions to a temporary inactive state nor (2) a fluorophore transitions from a temporary inactive state to a fluorescing state is given by the product

$$P(0|M,N) = P(0|M)P(0|N) = (1-\lambda_M)^{M}(1-\lambda_N)^{N}. \tag{S24}$$

The probability that only one fluorophore transitions is

$$P(1|M,N) = P(1|M)P(0|N) + P(0|M)P(1|N). \tag{S25}$$

The probability that only one fluorophore out of $M + N$ fluorophores transitions during Δt can then be

calculated using Eq. S22. Similar expressions can be derived for the case of diffusion-based and transient labeling (as in PAINT), but since the rates are easily controlled empirically by changing fluorophore concentration in solution, expressions are not derived here.

We wished to validate the above equations using simulated fluorophore transitions. For $\Delta t = 0.1$ s, $\tau_{pb} = \infty$ s, τ_{pi} = 10 s, and τ_{pa} = 1 s, M = 2, and N = 18, 84.6% of the frames that show transitions are expected to only show one transition. This was corroborated with a Monte Carlo fluorophore simulation in which 20 fluorophores started in the actively fluorescing state and were allowed to evolve for 10000 frames (0.1 s per frame). In this case, the percent of frames with transitions that showed only one transition was 84.5%.

Plotting super-resolution images. Although we developed software for representing the super-resolution data in several ways, unless otherwise specified, the super-resolution images in this article were plotted in the following manner. Individual spot fits were plotted as two-dimensional Gaussian functions, integrated over the area of the plot pixel (see eq. [S9]). The length of the side of a pixel in the super-resolution image was usually chosen to be 10 nm (all figures in this article used 10 nm). The center of the Gaussian was given by the fit parameters (x_0, y_0). The width of the Gaussian, σ (see eq. [S9]), was the average of the estimated errors (given by the Cramér-Rao lower bound [CRLB]) for the x_0 and y_0 estimates. The Gaussian was normalized to a volume-under-the-curve equal to 1000. To speed up plotting, the Gaussians were only plotted within a square with sides equal to 8σ and centered on the pixel containing (x_0, y_0). For positions > 4σ from the center of the Gaussian, the values of the Gaussian function were considered negligible.

SUPPLEMENTARY TABLES

Table S1. Algorithm parameters and fitting results for data presented in Figure 2c.

Detection parameters and criteria	
Image dilation iterations	2
Spot detection integration radius	3 pixels
Threshold (average within integration radius)	29 photons
Detection results	
Photobleaching events	22491
Photoactivation events	21080
Fitting parameters	
Maximum allowed error	0.5 pixels
Minimum σ	1 pixel
Maximum σ	2 pixels
Maximum A	500 photons
Fitting results (non-rejected spot fits)	
Photobleaching events	6530
Photoactivation events	6618

Table S2. Algorithm parameters and fitting results for data presented in Figure 3b.

Detection parameters and criteria	
Image dilation iterations	2
Spot detection integration radius	3 pixels
Threshold (average within integration radius)	67 photons
Detection results	
Photobleaching events	54835
Photoactivation events	49752
Fitting parameters	
Maximum allowed error	0.5 pixels
Minimum σ	1 pixel
Maximum σ	2 pixels
Maximum A	1000 photons
Fitting results (non-rejected spot fits)	
Photobleaching events	22262
Photoactivation events	22137

Table S3. Algorithm parameters and fitting results for data presented in Figure 4b.

Detection parameters and criteria	
Image dilation iterations	2
Spot detection integration radius	3 pixels
Threshold (average within integration radius)	5 photons
Detection results	
Photobleaching events	4518
Photoactivation events	4315
Fitting parameters	
Maximum allowed error	0.5 pixels
Minimum σ	1 pixel
Maximum σ	1.8 pixels
Maximum A	150 photons
Fitting results (non-rejected spot fits)	
Photobleaching events	1104
Photoactivation events	1210

Table S4. Algorithm parameters and fitting results for data presented in Figure 4e.

Detection parameters and criteria	
Image dilation iterations	2
Spot detection integration radius	3 pixels
Threshold (average within integration radius)	84 photons
Detection results	
Photobleaching events	14771
Photoactivation events	14262
Fitting parameters	
Maximum allowed error	0.5 pixels
Minimum σ	1 pixel
Maximum σ	2 pixels
Maximum A	1200 photons
Fitting results (non-rejected spot fits)	
Photobleaching events	10519
Photoactivation events	10292

Table S5. Algorithm parameters and fitting results for data presented in Figure 5b.

Detection parameters and criteria	
Image dilation iterations	2
Spot detection integration radius	3 pixels
Threshold (average within integration radius)	7 photons
Detection results	
Photobleaching events	2435887
Photoactivation events	2417237
Fitting parameters	
Maximum allowed error	0.5 pixels
Minimum σ	0.8 pixel
Maximum σ	2 pixels
Maximum A	100 photons
Fitting results (non-rejected spot fits)	
Photobleaching events	215467
Photoactivation events	221136

Table S6. Results of fluorophore localization using maximum-likelihood-based two-dimensional Gaussian fitter for a simulated, blinking fluorophore on a varying, uniform background. The fluorophore was simulated as a Gaussian function with peak intensity = 500 photons.

Detection parameters and criteria		
	Image dilation iterations	2
	Spot detection integration radius	3 pixels
	Detection threshold value	87 photons
Fitting criteria		
	Maximum allowed error	0.5 pixels
	Minimum σ	1 pixel
	Maximum σ	2 pixels

Background	Detected photobleaching events	Detected photoactivation events	Well-fit photobleaching events	Well-fit photoactivation events	Observed σ_{x0}	Average of CRLB error estimates	Estimated Thompson et al. error
0	500	500	499	499	0.037	0.019	0.018
1	500	500	500	500	0.020	0.019	0.018
10	500	500	500	500	0.023	0.022	0.019
25	500	500	500	500	0.025	0.024	0.020
40	500	500	500	500	0.027	0.026	0.021
50	500	500	500	500	0.028	0.028	0.021
60	500	500	500	500	0.030	0.029	0.022
75	501	500	499	500	0.029	0.030	0.023
100	500	500	500	500	0.032	0.033	0.024
500	501	501	499	499	0.058	0.058	0.040
1000	502	501	498	499	0.080	0.078	0.054
5000	508	507	493	493	0.170	0.168	0.114
7500	533	536	467	468	0.211	0.207	0.139
10000	590	579	431	430	0.252	0.240	0.161
12500	625	660	409	388	0.289	0.263	0.179
14000	694	717	367	363	0.349	0.274	0.190
15000	722	765	350	338	0.331	0.283	0.196
16000	749	759	350	354	0.676	0.298	0.203
17500	852	860	294	323	0.624	0.301	0.212
20000	966	915	289	294	0.856	0.324	0.226

Table S7. Results of fluorophore localization using maximum-likelihood-based two-dimensional Gaussian fitter for a simulated, blinking fluorophore on a uniform background and a nearby, non-blinking fluorophore. The simulated fluorophore was centered at $(x_0, y_0) = (10.5, 10.5)$.

Detection parameters and criteria		
	Image dilation iterations	2
	Spot detection integration radius	3 pixels
	Detection threshold value	87 photons
Fitting criteria		
	Maximum allowed error	0.5 pixels
	Minimum sigma	1 pixel
	Maximum sigma	2 pixels

2nd fluorophore's peak intensity	Detected photobleaching events	Detected photoactivation events	Well-fit photobleaching events	Well-fit photoactivation events	Average x_0	x_0 standard deviation	Average of CRLB error estimates
0	501	500	499	500	10.500	0.032	0.033
500	500	501	500	499	10.504	0.043	0.044
1000	503	501	497	499	10.503	0.054	0.053
5000	501	501	499	499	10.500	0.099	0.095
10000	506	505	494	495	10.495	0.131	0.130
20000	507	506	488	490	10.499	0.199	0.180
50000	506	505	405	410	10.507	0.316	0.274

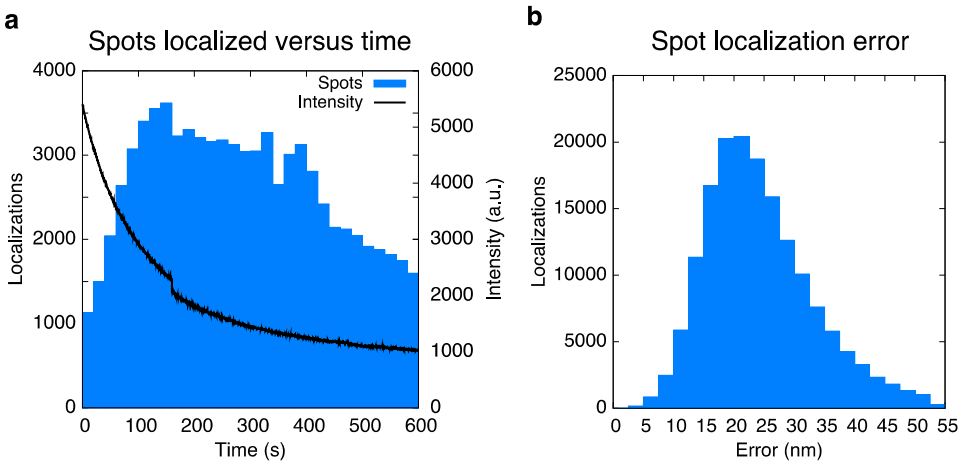

Figure S1. Additional information for Fig. 2d. (a) Spots localized per unit time increases as the microtubules photobleach to an optimal labeling density (in this case, one active fluorophore per 14 nm length of microtubule) and then decreases as the system is depleted of active fluorophores. A small discontinuity in the frame intensity occurs near 150 s due to an interruption in data acquisition. Bin width = 20 frames = 4 s. (b) Distribution of per-spot localization errors for spots plotted in a final super-resolution image. Bin width = 2.5 nm.

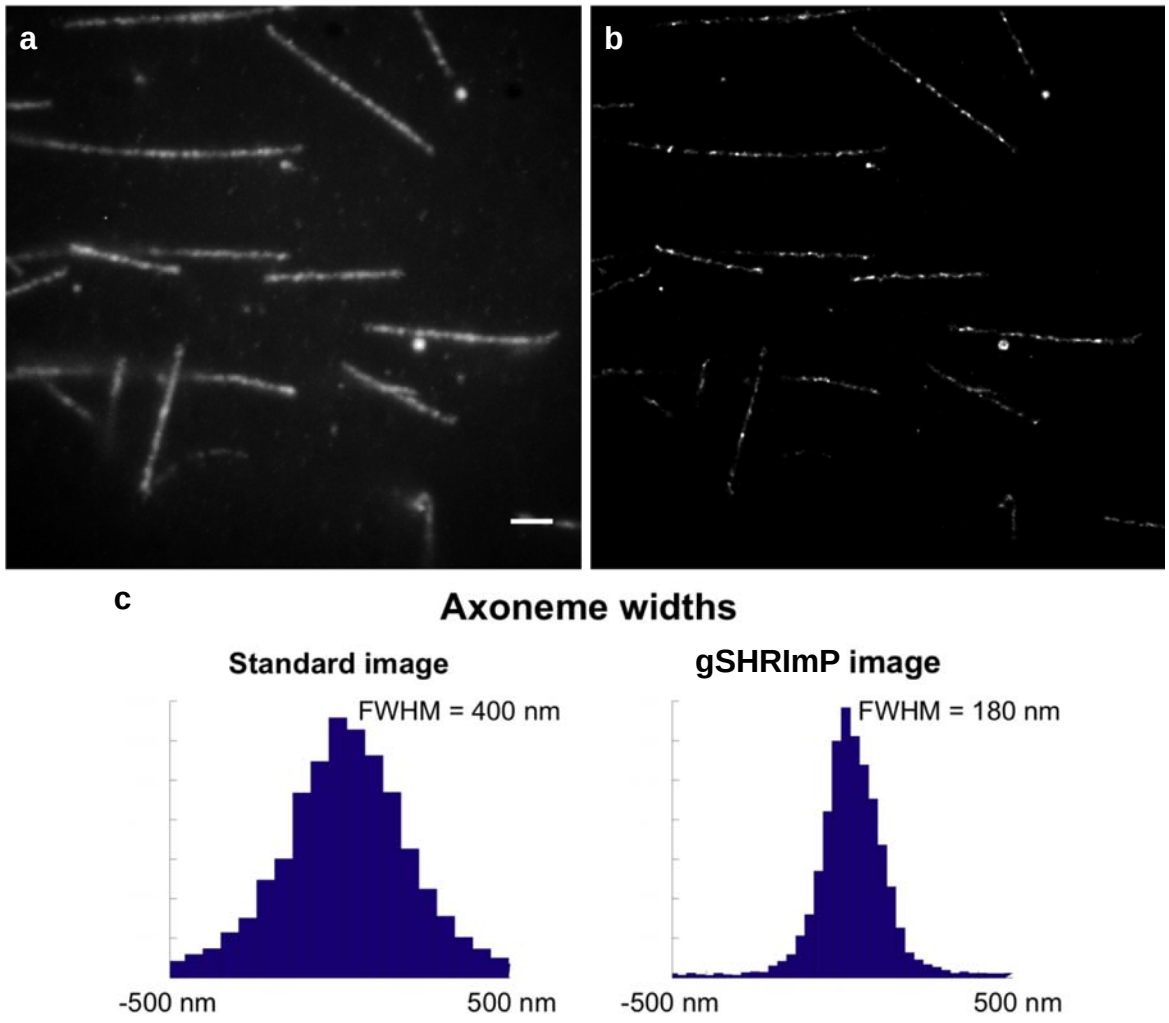

Figure S2. (a) Tetramethylrhodamine-labeled axonemes on glass and imaged using epifluorescence. (b) gSHRImP image. Scale bar = 1 μm. (c) Axoneme widths in normal and gSHRImP images. Segments of axonemes from (a) and (b) were fit to straight lines, and the distribution of fluorescence perpendicular to the long axes of the axonemes was plotted to find the apparent width. 11 segments, each near 5 μm in length, were fit this way to produce these plots.

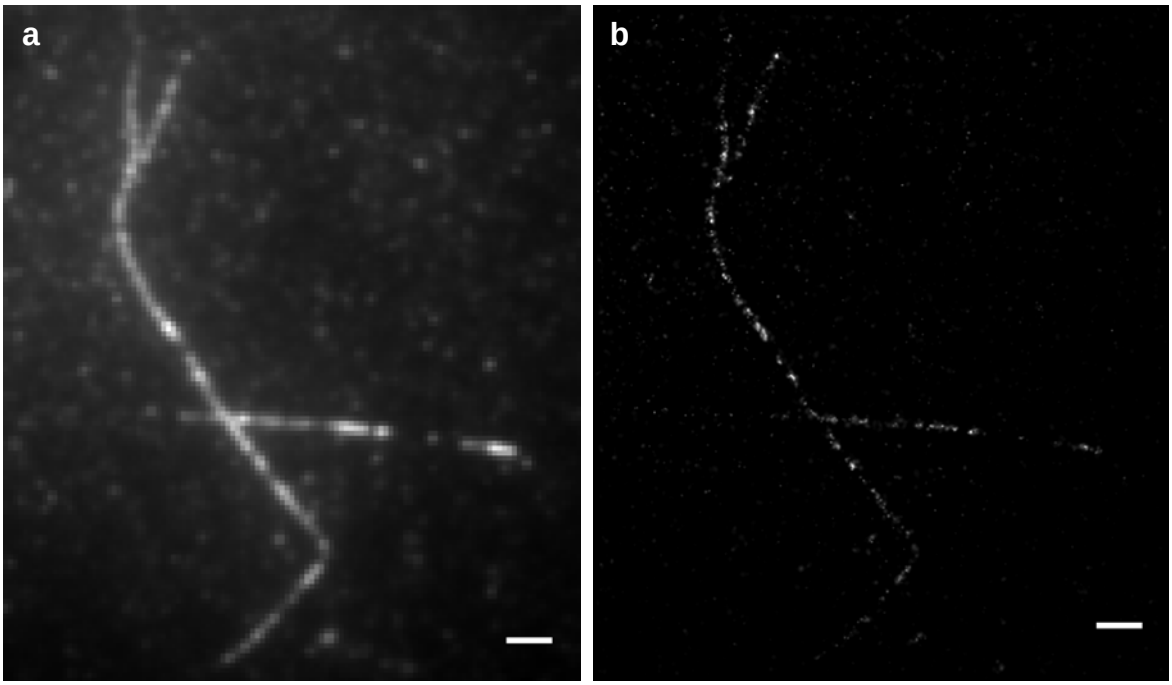

Figure S3. Lamda DNA on glass and labeled diffusively with SYTO. (a) Average of frames of movie. (b) Result of gSHRImP analysis. In these images, drift correction was *not* used. Scale bar = 1 μm.

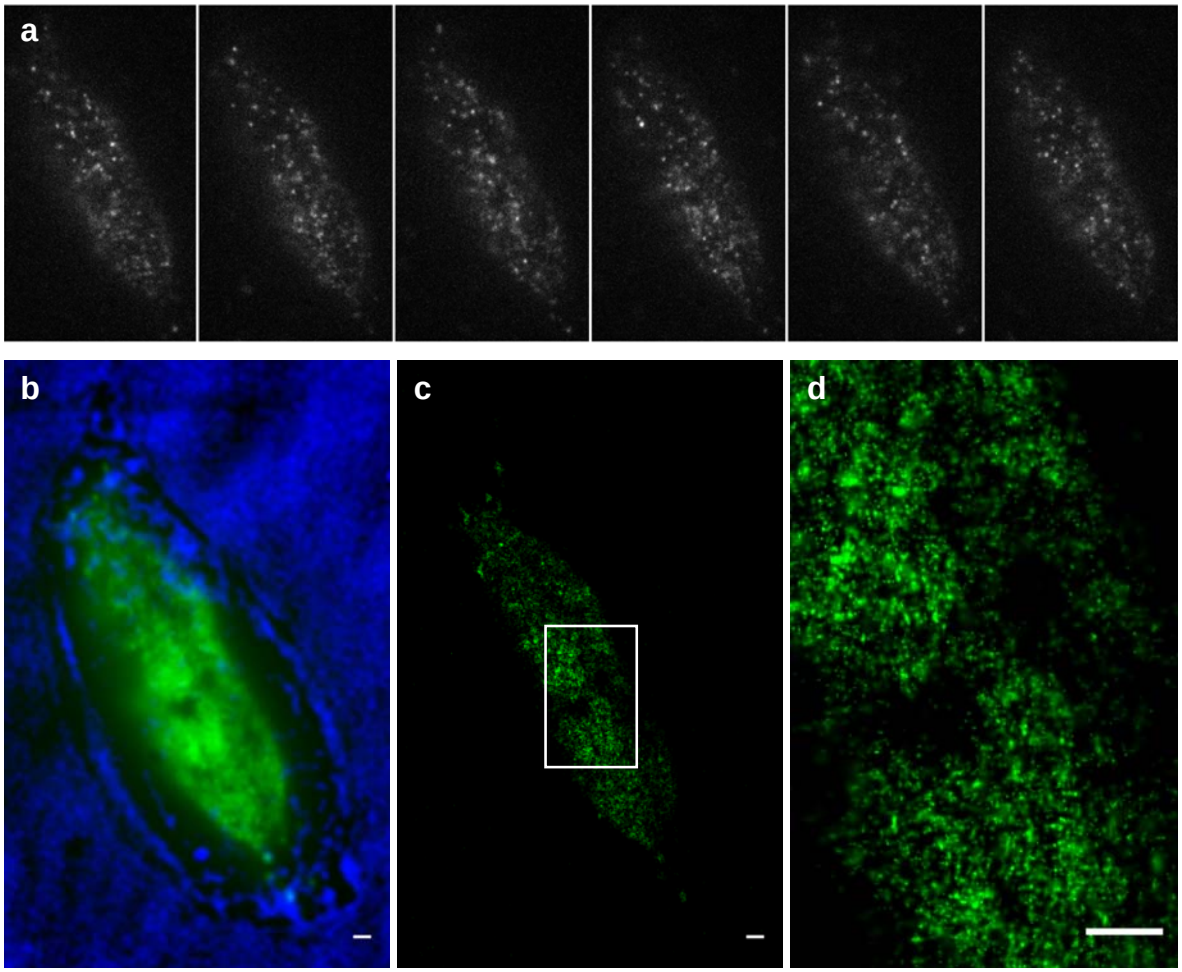

Figure S4. Super-resolution imaging of DNA in a HEK cell. DNA was labeled using a dilute solution of SYTO 16 dye. (a) Image sequence with single frames selected at 199-frame intervals. (b) Average of all fluorescence imaging frames (green) merged with a brightfield image of the cell showing the outline of the cell (blue). (c) gSHRImP image. Average spot localization error was 24 nm. (d) Zoomed-in portion of part (c). The gSHRImP image was constructed from 1000 image frames, 0.2 s per frame. Scale bar = 1 μm.

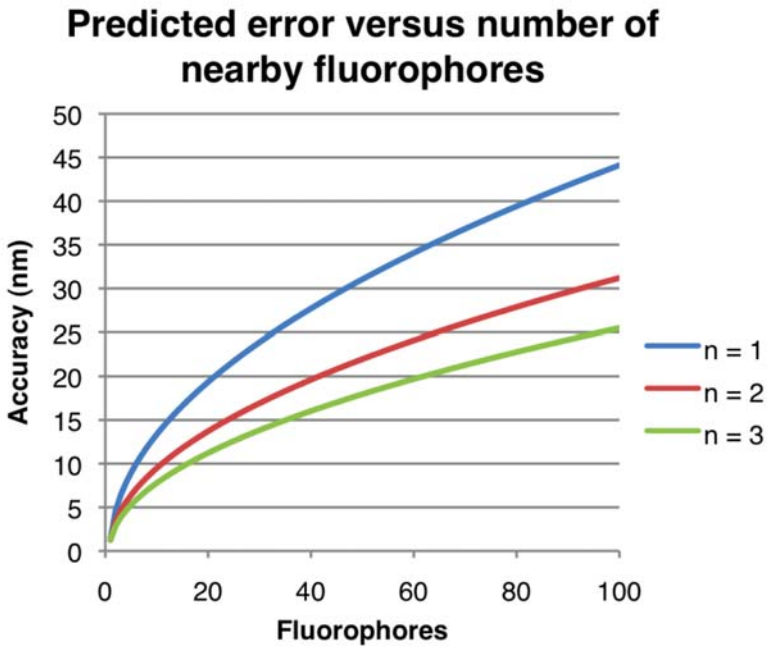

Figure S5. Equation (S5) estimates the localization error that can be achieved when there are several fluorophores crowded into a diffraction-limited area. The plot shows the predicted accuracy for s = 125 nm, a = 100 nm, and N = 10,000 photons. Increasing frame averaging, where n is the number of frames averaged before and after a photobleaching event occurs, allows for smaller localization errors.

SUPPLEMENTARY REFERENCES

1. Thompson, R. E.; Larson, D. R.; Webb, W. W., *Biophys. J.* **2002,** *82* (5), 2775-83.

2. Aitken, C. E.; Marshall, R. A.; Puglisi, J. D., *Biophys. J.* **2008,** *94* (5), 1826-35.

3. Hyre, D. E.; Le Trong, I.; Freitag, S.; Stenkamp, R. E.; Stayton, P. S., *Protein. Sci.* **2000,** *9* (5), 878-85.

4. Howarth, M.; Chinnapen, D. J.; Gerrow, K.; Dorrestein, P. C.; Grandy, M. R.; Kelleher, N. L.; El-Husseini, A.; Ting, A. Y., *Nat. Methods* **2006,** *3* (4), 267-73.

5. Lemons, D. S.; Langevin, P., *An introduction to stochastic processes in physics : containing "On the theory of Brownian motion" by Paul Langevin, translated by Anthony Gythiel*. Johns Hopkins University Press: Baltimore, 2002; p xii, 110 p.

6. Taylor, J. R., *An Introduction to Error Analysis: the Study of Uncertainties in Physical Measurements*. University Science Books: Sausalito, California, 1997; Vol. 327.

7. Bos, A. v. d., *Parameter estimation for scientists and engineers*. Wiley-Interscience: Hoboken, N.J., 2007; p xiv, 273 p.

8. Smith, C. S.; Joseph, N.; Rieger, B.; Lidke, K. A., *Nat. Methods* **2010,** *7* (5), 373-375.

9. Ober, R. J.; Ram, S.; Ward, E. S., *Biophys. J.* **2004,** *86* (2), 1185-200.